Visualizing Peroxynitrite Fluxes in Endothelial Cells Reveals the Dynamic Progression of Brain Vascular Injury

ARTICLE *in* JOURNAL OF THE AMERICAN CHEMICAL SOCIETY · SEPTEMBER 2015

Impact Factor: 12.11 · DOI: 10.1021/jacs.5b06865

JACS
JOURNAL OF THE AMERICAN CHEMICAL SOCIETY

Article

pubs.acs.org/JACS

Visualizing Peroxynitrite Fluxes in Endothelial Cells Reveals the Dynamic Progression of Brain Vascular Injury

Xin Li,[†,∥] Rong-Rong Tao,[‡,∥] Ling-Juan Hong,[‡] Juan Cheng,[†] Quan Jiang,[‡] Ying-Mei Lu,[§] Mei-Hua Liao,[‡] Wei-Feng Ye,[‡] Nan-Nan Lu,[‡] Feng Han,*[,‡] Yong-Zhou Hu,*[,†] and You-Hong Hu*[,†]

[†]ZJU-ENS Joint Laboratory of Medicinal Chemistry, College of Pharmaceutical Sciences, Zhejiang University, Hangzhou 310058, China

[‡]Institute of Pharmacology and Toxicology, College of Pharmaceutical Sciences, Zhejiang University, Hangzhou 310058, China

[§]School of Medicine, Zhejiang University City College, Hangzhou 310015, China

Supporting Information

ABSTRACT: Accumulating evidence suggests that formation of peroxynitrite ($ONOO^-$) in the cerebral vasculature contributes to the progression of ischemic damage, while the underlying molecular mechanisms remain elusive. To fully understand $ONOO^-$ biology, efficient tools that can realize the real-time tracing of endogenous $ONOO^-$ fluxes are indispensable. While a few $ONOO^-$ fluorescent probes have been reported, direct visualization of $ONOO^-$ fluxes in the cerebral vasculature of live mice remains a challenge. Herein, we present a fluorescent switch-on probe (**NP3**) for $ONOO^-$ imaging. **NP3** exhibits good specificity, fast response, and high sensitivity toward $ONOO^-$ both in vitro and in vivo. Moreover, **NP3** is two-photon excitable and readily blood−brain barrier penetrable. These desired photophysical and pharmacokinetic properties endow **NP3** with the capability to monitor brain vascular $ONOO^-$ generation after injury with excellent temporal and spatial resolution. As a proof of concept, **NP3** has enabled the direct visualization of neurovascular $ONOO^-$ formation in ischemia progression in live mouse brain by use of two-photon laser scanning microscopy. Due to these favorable properties, **NP3** holds great promise for visualizing endogenous peroxynitrite fluxes in a variety of pathophysiological progressions in vitro and in vivo.

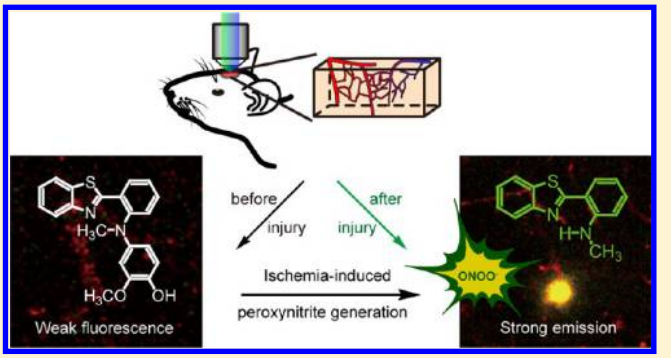

INTRODUCTION

Peroxynitrite ($ONOO^-$), a highly reactive nitrogen species generated from the reaction between nitric oxide (NO) and superoxide ($O_2^{\cdot-}$) at a diffusion-limited rate of 1.9×10^{10} $M^{-1}\cdot s^{-1}$ under pathological conditions,[1] attracts increasing attention due to its "double-edged" character.[2,3] $ONOO^-$ may exert a contributory effect by participating in nitrating tyrosine signaling.[4] Nevertheless, $ONOO^-$ is more frequently regarded as deleterious due to its nitrosative damage to lipids, proteins, and DNA.[5,6] $ONOO^-$ has been implicated in various redox-related diseases,[5,7,8] including ischemia-reperfusion injury.[9] We have been particularly interested in the roles of $ONOO^-$ in the progression of brain ischemia-induced endothelial dysfunction and neurovascular pathogenic cascades. Our preliminary results have shown that $ONOO^-$ is formed under conditions of ischemia and that its nitrosative damage is implicated in neurovascular damage following cerebral ischemia.[10−12] Traditional biological assay for $ONOO^-$ primarily relies on the immunostaining of 3-nitrotyrosine.[13] This method has the major limitation of being incompatible with living systems and can therefore no longer satisfy research needs for tracking native $ONOO^-$ in real time with high spatial resolution, which is pivotal for fully understanding $ONOO^-$ pathology in contexts of ischemia.

Fluorescence imaging employing small molecular probes, however, has emerged as a desirable and indispensable tool for interrogating intact living samples.[14,15] Due to the obvious technical and practical advantages of good membrane permeability, high sensitivity, and operational simplicity, fluorescence probes are attracting increasing attention in life science fields,[16−19] especially two-photon excitable probes, because they are compatible with two-photon fluorescence microscopy and can therefore realize three-dimensional imaging of biological specimens with deeper tissue penetration and less photodamage.[20−22] Indeed, several fluorescent probes are commercially available to detect $ONOO^-$, such as aminophenyl fluorescein (APF) and hydroxyphenyl fluorescein (HPF).[23] Unfortunately, these probes are limited by their poor selectivity for $ONOO^-$ against other highly reactive species, such as $^{\bullet}OH$ or ClO^-.[24] To address this problem, several research groups have set out to develop new probes, and this

Received: July 2, 2015

DOI: 10.1021/jacs.5b06865
J. Am. Chem. Soc. XXXX, XXX, XXX−XXX

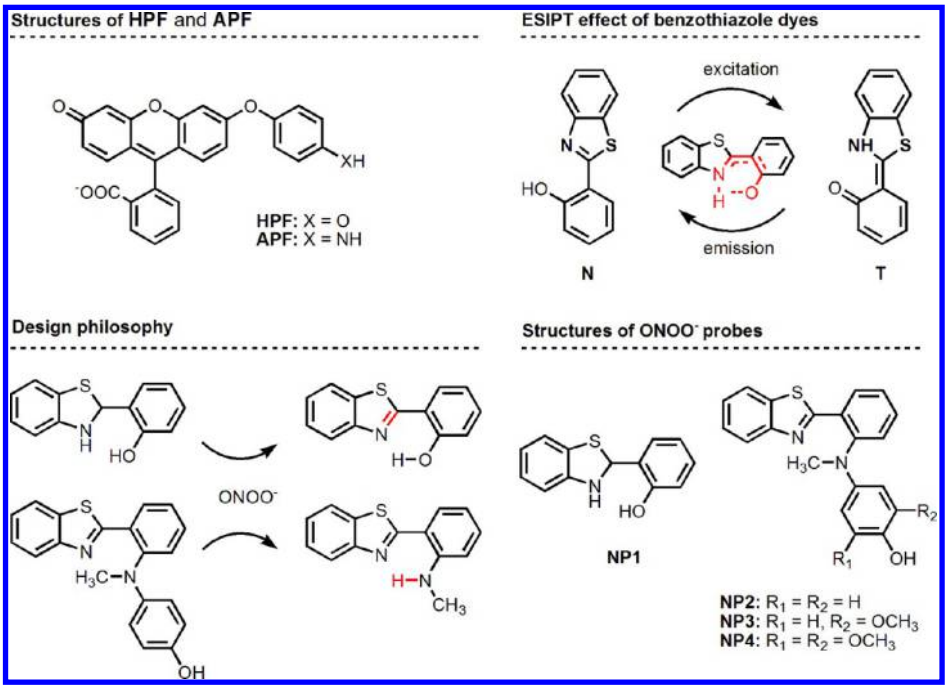

Figure 1. Structures of BT series of $ONOO^-$ probes and design philosophy.

elegant work has resulted in the development of several selective probes suitable for imaging $ONOO^-$ in live cells,[25−37] live mice,[30] or even the redox cycles between $ONOO^-$ and glutathione.[30,32,38] Facilitated by these probes, visualization of $ONOO^-$ in macrophages during immune response[25−27,29,30,32,33,35] or in mouse hearts under atherosclerosis[26] has been realized. However, study on the real-time visualization of $ONOO^-$ production in the brain of live animals with ischemia-induced neurovascular damage is still lacking, which represents a great challenge due to the rigid requirements for brain imaging agents including high specificity, desired photophysical properties, and good blood−brain barrier (BBB) penetrability.[39,40]

Herein, we report a two-photon fluorescent "switch-on" probe for the detection of $ONOO^-$. The probe, judiciously designed by combining the basic principles of fluorescent probe design and drug design, is highly specific and sensitive toward $ONOO^-$, two-photon excitable, and most importantly, readily BBB-penetrable. It is fluorescence-silent in the absence of $ONOO^-$ but can respond rapidly to $ONOO^-$ with dramatic emission enhancement (utmost 600-fold). Its capability to track in situ generation of $ONOO^-$ in live cells and live mice with ischemia-induced neurovascular damage has been fully characterized.

RESULTS AND DISCUSSION

Probe Design and Synthesis. To image $ONOO^-$ in live animals, the fluorophore selected for probe construction should be nontoxic, sufficiently bright, inert to other species in the complex biological context, excitable with deep-penetrating infrared light, and possess desired pharmacokinetic profiles. Among the prevalent fluorescent markers for bioimaging, 2-(2′-hydroxyphenyl)benzothiazole (BT) provoked our interest due to its druglike physical−chemical performance and good photophysical properties. First, the benzothiazole skeleton may exhibit the desired pharmacokinetic properties, especially the BBB penetration ability mandatory for brain imaging agents, as exemplified by [^{11}C]PIB, an extensively studied positron emission tomography imaging probe for Aβ plaques in humans.[41] Second, the BT series of fluorophores commonly exist in the normal form (N) with weak fluorescence but can automerize under excitation (T) via a process called excited-state intramolecular proton transfer (ESIPT) (Figure 1),[42] accompanied by both enhancement and red shift of their fluorescence. Blockage of this ESIPT effect with a special chemical motif that can react selectively with intended target in complex biological milieu to initiate the ESIPT process enables the design of sensitive fluorescent probes. Third, BT fluorophore is two-photon excitable and may be compatible with live tissue imaging.[43] With all these considerations, probe **NP1** was designed by blocking the ESIPT process with a saturated C−N bond (Figure 1). We envisioned that the great tendency to be aromatic would render **NP1** susceptible to oxidation by $ONOO^-$ and therefore restore the ESIPT process. **NP1**, as anticipated, could indeed respond to $ONOO^-$ with a swift fluorescence intensity enhancement in phosphate-buffered saline (PBS; 10 mM, pH 7.4) (Figures S1 and S2). However, **NP1** was found to be unstable when exposed to air. This instability challenges its selectivity. To develop probes with improved stability and specificity, we next blocked the hydrogen donor of the ESIPT process and designed **NP2** by switching the hydroxyl group to *N*-methyl-*p*-hydroxyaniline, where the phenol group may be oxidized to benzoquinone by $ONOO^-$, accompanied by N−C (sp^2) bond cleavage, thereby furnishing a proton donor (Figure 1).[26] **NP3** and **NP4** were also designed by installing electron-donating groups to the *p*-hydroxyaniline ring in order to make the hydroxyl group more susceptible to oxidants. All the probes were facilely synthesized via Mills reaction (Scheme S1).

Probe Evaluation. We first tested the fluorescence responses of **NP2−4** toward $ONOO^-$. These probes (5.0 μM) alone were nearly nonemissive in PBS. In contrast, in the presence of $ONOO^-$ (10 μM), all showed obvious fluorescence enhancement, and **NP3** was the most sensitive one with an

DOI: 10.1021/jacs.5b06865
J. Am. Chem. Soc. XXXX, XXX, XXX−XXX

increase factor of 600-fold, followed by **NP2** and **NP4** (Figure S3). These results not only distinguish **NP3** as a desirable candidate for further study but also suggest that both electronic and steric effects should be considered for probe design because the steric effects of the methoxy groups adjacent to the hydroxyl group in **NP4** greatly outweigh their positive electron-donating effects.

Spectroscopic Properties and Selectivity. To profile the response of **NP3** toward $ONOO^-$ in detail, we examined its specificity by recording its responses toward various reactive oxygen species (ROS) and reactive nitrogen species (RNS). Encouragingly, no analytes other than $ONOO^-$ could switch on the fluorescence of **NP3**. **NP3** could still recognize $ONOO^-$ with a dramatic increase in fluorescence intensity even in the presence of other reactive species, cations, or amino acids commonly found in biological systems, implying great specificity of **NP3** toward $ONOO^-$ (Figure 2a and Figure S4).

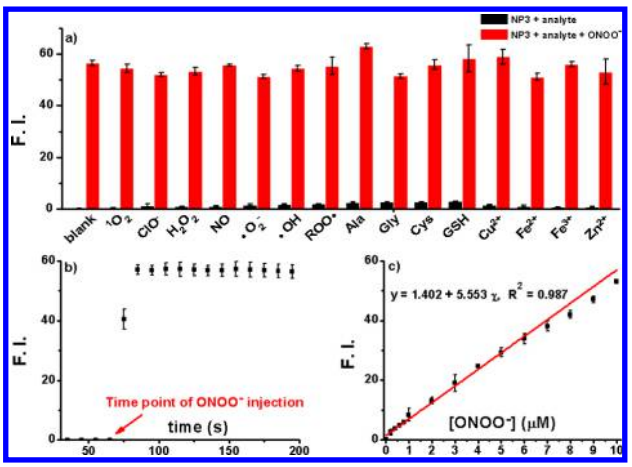

Figure 2. Characterization of fluorescent response of **NP3** toward $ONOO^-$. (a) Fluorescent responses of **NP3** (5 μM) toward various analytes (10 μM). Data shown represent fluorescent intensity at 470 nm, 30 min after addition of various analytes. (b) $ONOO^-$ (final concentration 10 μM) was quickly injected into a solution of **NP3** (final concentration 5 μM), and the fluorescent intensity at 470 nm was plotted against time. (c) Fluorescence enhancement of **NP3** (5 μM) at 470 nm as a function of $ONOO^-$ (0–10 μM) after 15 min of reaction. All data were acquired in PBS (10 mM, pH 7.4) with excitation at 375 nm.

Next, the sensing kinetics was studied, and the reaction between **NP3** and $ONOO^-$ was found to be completed within seconds (Figure 2b and Figure S5), which is important given the extremely elusive nature of $ONOO^-$. Moreover, the fluorescence enhancement of **NP3** was linearly correlated with concentrations of $ONOO^-$ ranging from 0 to 10 μM, implying the great potential of **NP3** to quantify $ONOO^-$ (Figure 2c and Figure S6). The detection limit of **NP3** was as low as 5.0 nM (S/N = 3) (Figure S7). Notably, $ONOO^-$ detection by **NP3** was insusceptible to pH changes in the surroundings (Figure S8). Additionally, sufficient photostability was observed for both **NP3** and the detection system (Figure S9), indicating the robustness of **NP3**.

We also evaluated the ability of **NP3** to detect $ONOO^-$ in two-photon excitation mode by measuring fluorescence spectra of the **NP3**–$ONOO^-$ mixture with two-photon excitation. As expected, sensitive signals remained. The two-photon absorption cross sections (σ) of the system at 760–820 nm were also determined with fluorescein in H_2O (pH = 13) as standard,[44] and σ_{max} was observed at 820 nm with a value of 3.6 GM (Figure S10). These results firmly support the feasibility of **NP3** as a highly specific and sensitive probe for $ONOO^-$ in vitro that shows promise for in vivo imaging.

In agreement with the fluorescence switch-on response, treating **NP3** (10 μM) with $ONOO^-$ could also induce a dramatic change in its UV absorption profile. **NP3** itself exhibited a major absorption band centered at 300 nm (ε 16 310), whereas $ONOO^-$ treatment resulted in the disappearance of this band and the appearance of two new bands centered at 285 and 350 nm, both of which strengthened in a $ONOO^-$ concentration-dependent manner (Figure S11), indicating removal of the phenol ring and generation of an intramolecular hydrogen bond as shown in Figure 1. We also verified the detection mechanism by isolating and characterizing the reaction product by ^1H NMR and HRMS spectral analysis (Figures S12 and S13).[45]

Determination of Plasma and Brain NP3 Concentrations. Pharmacokinetic study in C57 mice showed that **NP3** readily crossed the blood–brain barrier (Figure S14). A 1.3-fold brain/plasma ratio was achieved after 0.5 h of tail intravenous (iv) injection dosing at 10 mg/kg. The absolute brain concentration reached a high level of 970 ng/mL at 0.5 h after **NP3** administration and only 136 ng/mL remained after 2 h, indicating the efficient brain penetration and fast brain clearance rate of **NP3**, which are deemed advantageous for brain imaging agents.

Fluorescent Response of NP3 to Dynamic Changes in Nitrosative Stress in Live Endothelial Cells. With the photophysical profiles of **NP3** fully characterized, we next investigated its feasibility for dynamically tracking intracellular $ONOO^-$ generation. A time-lapse series of single confocal plane images were taken to observe the **NP3** fluorescence response toward $ONOO^-$ in live EA.hy926 endothelial cells after incubation with or without 3-morpholinosydnonimine (SIN-1, 0.5 mM), an $ONOO^-$ donor. As shown in Figure 3, no detectable fluorescence signal was observed in endothelial cells loaded with **NP3** in the absence of the $ONOO^-$ donor SIN-1 (Figure 3a,b). However, upon exposure to SIN-1, intracellular fluorescence in endothelial cells gradually increased 10 min after SIN-1 stimulation and kept increasing in a time-dependent manner until at least 50 min after treatment (Figure 3a,b). In contrast, clearance of $ONOO^-$ with uric acid (100 μM) or 5,10,15,20-tetrakis(4-sulfonatophenyl)porphyrinatoiron(III) chloride (FeTTPS; 1 μM) blunted the robustness of **NP3** fluorescence in $ONOO^-$-treated endothelial cells (Figure 3c and Figures S15 and S16). **NP3** also worked well as an efficient $ONOO^-$ probe in other cell lines, as shown in human brain microvascular endothelial cells (HBMEC) in Figure S17. The $ONOO^-$ (Figure S17a) or SIN-1 (Figure S17b) treatment-induced **NP3** fluorescence elevation was also observed in a dose-dependent manner in HBMEC. These results indicate that **NP3** is applicable for real-time tracking of $ONOO^-$ generation in live cells and suggest its promise for serving as a molecular imaging tool to explore $ONOO^-$ biology under pathological conditions.

Visualizing $ONOO^-$ Fluxes in Endothelial Cells after Oxygen–Glucose Deprivation. Considerable evidence has indicated that $ONOO^-$ overproduction in endothelial cells mediates cellular damage during cerebral ischemia.[46–48] Thus, it would be interesting if **NP3** could help to identify dynamic changes of $ONOO^-$ formation during endothelial ischemic injury. As shown in Figure 4a, time-dependent accumulation of

DOI: 10.1021/jacs.5b06865
J. Am. Chem. Soc. XXXX, XXX, XXX–XXX

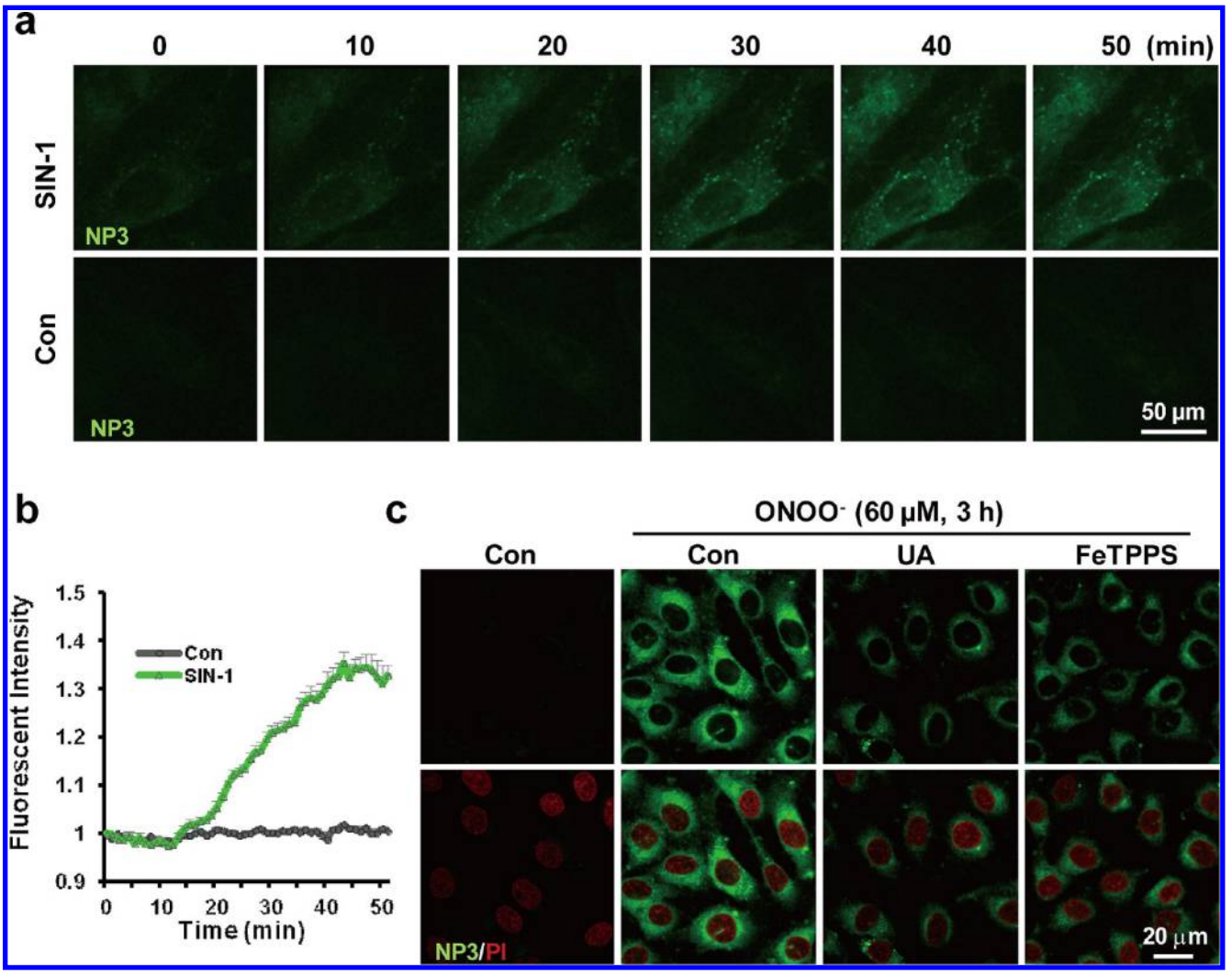

Figure 3. Characterization of $ONOO^-$ formation by **NP3** in endothelial cells upon nitrosative stress. (a) Time-lapse series of single confocal plane images taken from living EA.hy926 endothelial cells. The cells were seeded on glass-bottom 6-well plates overnight and then preincubated with **NP3** (5.0 μM) for 30 min, followed by stimulation with or without SIN-1 (0.5 mM). (b) Quantitative analysis of dynamic changes of **NP3** fluorescence after SIN-1 (0.5 mM) treatment in panel a. Data are presented as a densitometric ratio change compared with control. (c) Effects of $ONOO^-$ scavengers uric acid (100 μM) and FeTTPS (1 μM) on changes in **NP3** fluorescence in endothelial cells in the presence of $ONOO^-$ (60 μM). The $ONOO^-$ scavengers were preincubated for 1 h prior to $ONOO^-$ loading. Propidium iodide (PI) counterstaining indicates nuclear localization (red; λ_{ex} 543 nm, λ_{em} 560–615 nm). **NP3** fluorescence was collected at 420–480 nm with λ_{ex} 405 nm.

NP3 fluorescence was observed in endothelial cells over 0.5–2 h following oxygen–glucose deprivation (OGD) exposure. A similar pattern of fluorescence was observed in HBMEC (Figure 4b). To elaborate the specificity of **NP3** toward $ONOO^-$ during OGD treatment, FeTTPS (1 μM), the $ONOO^-$ decomposition catalyst, blunted the elevation of **NP3** fluorescence in OGD-treated endothelial cells (Figure 4c and Figures S18 and S19), confirming that **NP3** is specific for $ONOO^-$ during OGD insult. $ONOO^-$-mediated stress can also be initiated by early intracellular Ca^{2+} release and calmodulin activation.[49] To discern whether the OGD-induced increase of **NP3** fluorescence occurs in a Ca^{2+}/calmodulin-dependent manner, calmodulin inhibitors (W7 and melatonin) and a Ca^{2+}-specific aminopoly(carboxylic acid) [1,2-bis(*o*-aminophenoxy)ethane-*N*,*N*,*N*′,*N*′-tetraacetic acid, BAPTA] were used to bind Ca^{2+}/calmodulin signaling. As shown in Figure 4c and Figure S19, the OGD-induced increase of **NP3** fluorescence was reduced in the presence of either calmodulin inhibitor or BAPTA. Taken together, these results suggest that **NP3** is a highly selective and specific probe for monitoring $ONOO^-$ fluxes during ischemia.

Real-Time Monitoring of Vascular Peroxynitrite Fluxes with High Temporal and Spatial Resolution in Live Cells. Mitochondria constitute a primary locus for intracellular $ONOO^-$ formation and targeting.[50] For example, modification of tyrosine residues by endogenous $ONOO^-$ results in inhibition of mitochondrial complex I.[51] To further visualize the subcellular distribution of $ONOO^-$ labeled by **NP3** fluorescence, MitoRed (Invitrogen) was used to localize mitochondrial components in endothelial cells. **NP3** fluorescence in control endothelial cells was undetected (Figure 5 and Figure S20). Interestingly, consistent with MitoRed localization, elevated **NP3** fluorescence in endothelial cells after OGD was primarily observed to localize in the same components (Figure 5). Analysis of **NP3** fluorescence (green) in mitochondrial components of endothelial cells revealed a significant elevation after 1 h of OGD, and continuous elevation could be observed after 2 h until at

DOI: 10.1021/jacs.5b06865
J. Am. Chem. Soc. XXXX, XXX, XXX–XXX

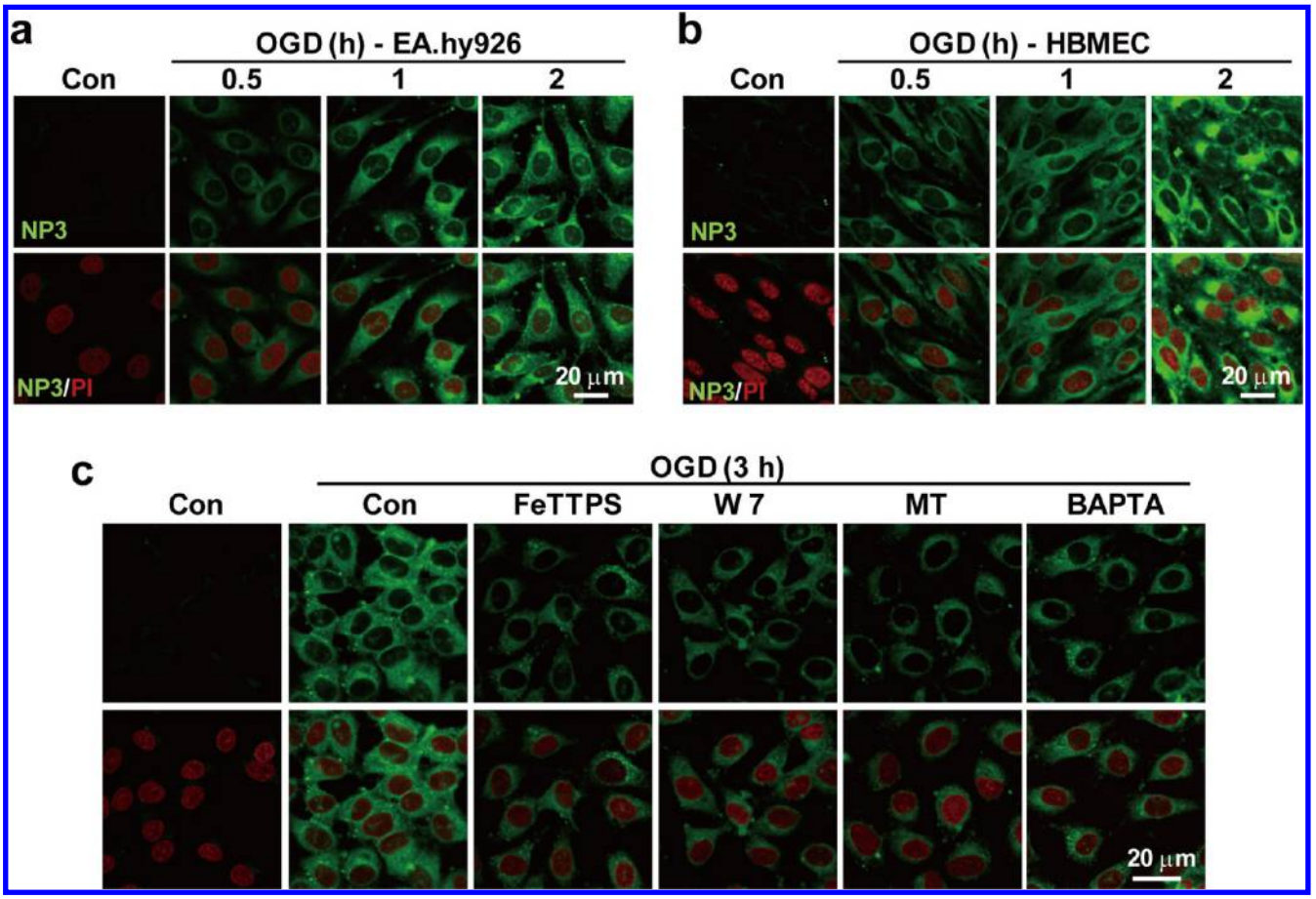

Figure 4. Characterization of $ONOO^-$ formation by use of **NP3** in endothelial cells upon OGD. (a, b) Representative confocal images show time-dependent accumulation of **NP3** fluorescence (green; λ_{ex} 405 nm, λ_{em} 420−480 nm) in (a) EA.hy926 endothelial cells over 0.5−2 h following OGD exposure as well as in (b) human brain microvascular endothelial cells (HBMEC). PI counterstaining indicated nuclear localization (red, λ_{ex} 543 nm, λ_{em} 560−615 nm). (c) The OGD-initiated **NP3** fluorescence response to $ONOO^-$ was modulated by suppressing $ONOO^-$ formation. EA.hy926 endothelial cells were pretreated with FeTTPS (1 μM), W7 (1 μM), melatonin (10 μM), or BAPTA (1 μM) 1 h prior to OGD treatment to suppress the $ONOO^-$ signal.

least 6 h (Figure 5 and Figure S20). Moreover, coinciding with the reports that lysosome response is also associated with nitrosative stress,[11,52] our results demonstrated that enhanced fluorescence is partially located in the lysosomal compartment (Figure S21), suggesting dynamic spatiotemporal coordination between $ONOO^-$ and lysosomes. Similar changes in **NP3** fluorescence were confirmed in HBMEC after OGD (Figures S22 and S23). The results indicated that **NP3** can monitor $ONOO^-$ flux during ischemic injury. Accompanied by increased **NP3** fluorescence in mitochondria, as well as the spreading distribution in endothelial cells, $ONOO^-$ accumulation challenged the endothelial cell and contributed to apoptosis, as shown by annexin V staining (blue), in agreement with the results that $ONOO^-$ could induce apoptosis (Figure S24). Thus, these collective data demonstrated that **NP3** efficiently visualized progressive $ONOO^-$ fluxes in endothelial cells with excellent temporal and spatial ability.

3-(4,5-Dimethylthiazol-2-yl)-2,5-diphenyltetrazolium bromide (MTT) assay showed that **NP3** did not exhibit cytotoxicity within 48 h except at such high concentrations as 150 and 200 μM (Figure S25). Moreover, the fairly low cytotoxicity of **NP3** was confirmed by mitochondrial membrane potential-sensing dye JC-1. Since the loss of mitochondrial transmembrane potential ($\Delta\Psi_m$) signals is a hallmark of mitochondrial dysfunction, cytotoxicity, and apoptotic signaling,[53] we used JC-1 to further investigate the potential cytotoxic effects of **NP3** on endothelial cells. No significant shift in JC-1 fluorescence from red to green was observed following **NP3** treatment up to 100 μM in EA.hy926 endothelial cells, compared with control cells undergoing JC-1 staining (Figure S26). Thus, these results suggest that **NP3** is nearly noncytotoxic up to 100 μM in endothelial cells, implying excellent biocompatibility for biological application, although further in vivo testing is necessary prior to application for clinical diagnosis.

Real-Time Imaging of Endogenous Peroxynitrite Formation after Brain Microvessel Injury in Live Mice. Combined with in vivo two-photon laser scanning microscopy (TPLSM), **NP3** enabled visualization of dynamic changes of neurovascular $ONOO^-$ formation upon ischemia in live mice. The ischemia mice were modeled by rose bengal-induced vascular occlusion[54] or laser irradiation-induced microvessel rupture.[55] The time series images in Figure 6 are individual frames from a continuous time-lapse movie. The dynamic elevation of local $ONOO^-$ formation (arrows) in the microvessel indicated by strong **NP3** fluorescence was efficiently monitored over a recording period of 30 s (Figure 6a and Movie S1). In contrast, no significant signal was observed in negative control experiments in which mice were modeled in the same way but not treated with **NP3**, indicating

DOI: 10.1021/jacs.5b06865
J. Am. Chem. Soc. XXXX, XXX, XXX−XXX

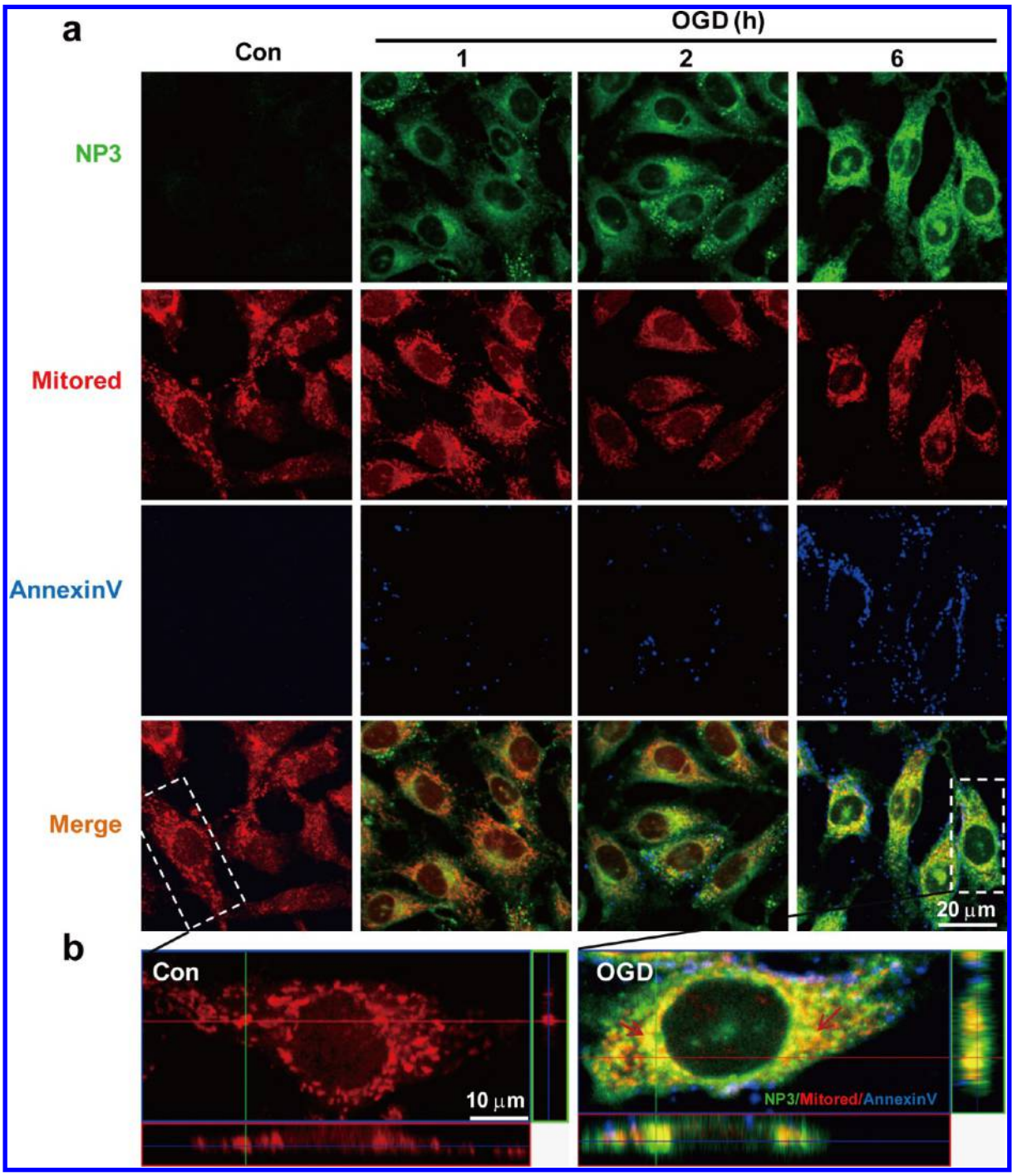

Figure 5. Distribution of **NP3** fluorescence, examined by counterstaining with the mitochondria indicator MitoRed after OGD. (a) Representative confocal images show temporal changes of $ONOO^-$-dependent **NP3** fluorescence (green; λ_{ex} 405 nm, λ_{em} 420−480 nm) and MitoRed (red; λ_{ex} 543 nm, λ_{em} 560−615 nm), as well as the apoptosis maker annexin V (blue; λ_{ex} 488 nm, λ_{em} 505−550 nm), following OGD treatment. (b) Orthogonal projections onto the $x-z$ (upper) and $y-z$ (right) planes are shown to confirm the colocalization of **NP3** and MitoRed throughout endothelial cells as shown in panel a after ischemia injury. All images were captured with a Zeiss LSM 510 confocal microscope.

the capacity of **NP3** for in vivo tracking of $ONOO^-$ fluxes during brain vascular damage (Figure S27).

Moreover, to provide another example of the in vivo-visualized $ONOO^-$ flux enabled by **NP3**, real-time imaging of endogenous $ONOO^-$ formation was performed in live mice suffering from laser irradiation-induced cerebrovascular rupture at the two-photon wavelength of 800 nm. As shown in Figure 6b, endogenous $ONOO^-$ formation increased dramatically upon laser irradiation-mediated microvessel injury at 10 s point and remained at its highest fluorescent intensity for at least 30 s (Figure 6b,c and Movie S2). Similar to our previously reported results that ischemia induced $ONOO^-$ production based on indirect evidence from immunoblot or immunostaining,[10,12] we observed laser irradiation-induced local $ONOO^-$ formation in injured cerebral microvessels in live mice using the combination of in vivo TPLSM and probe **NP3**. More importantly, we were able to visualize the dynamic changes of $ONOO^-$ formation in

DOI: 10.1021/jacs.5b06865
J. Am. Chem. Soc. XXXX, XXX, XXX−XXX

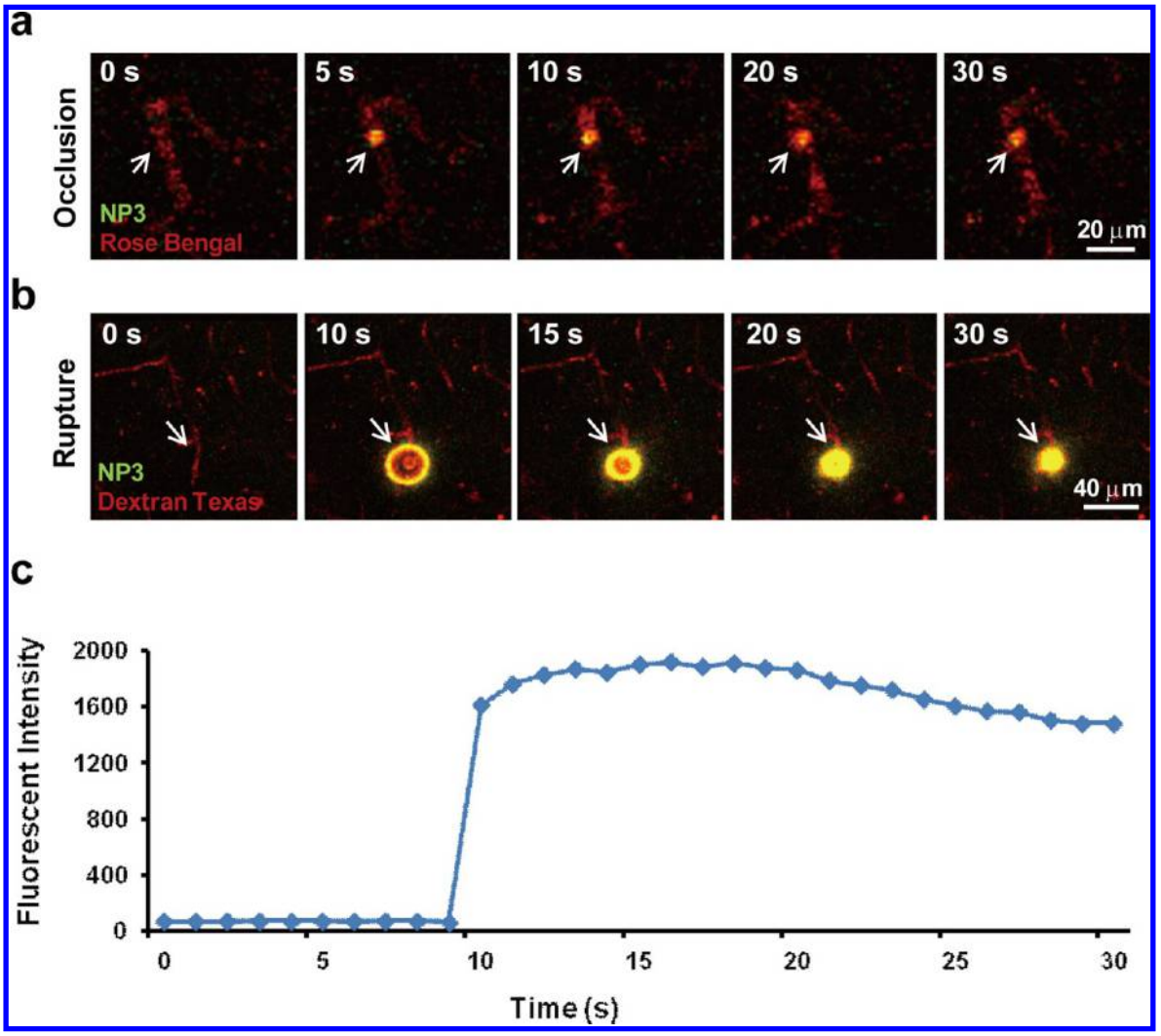

Figure 6. Real-time visualization of endogenous peroxynitrite fluxes after brain microvessel injury with a combination of **NP3** and in vivo two-photon laser scanning microscopy. For two-photon imaging, cortical brain vessels 10−15 μm in diameter and 100 μm below the cortical surface were selected for imaging. (a, b) The time-series images are individual frames from a continuous time-lapse movie and show dynamic **NP3** fluorescence elevation (arrows) following (a) rose bengal-induced vascular occlusion and (b) laser irradiation-induced vascular rapture in live mice. (c) Mean values of **NP3** fluorescence intensity from panel b were measured to quantify the progressive $ONOO^-$ formation in cerebrovessels after ischemia. Emission was collected at 420−480 nm for **NP3** fluorescence and 575−630 nm for dextran Texas or rose bengal upon excitation at 800 nm.

a temporal and spatial manner with high-resolution images in live mice.

CONCLUSION

To conclude, by considering basic principles of probe and drug design, we developed a fluorescent probe with desired pharmacokinetic and photophysical properties suitable for imaging of $ONOO^-$ generation in both live cells and live animals. The probe, designed by blocking the ESIPT process of the 2-(2′-hydroxyphenyl)benzothiazole fluorophore with a smart reaction trigger that readily undergoes bioorthogonal and specific reaction with $ONOO^-$ in biological contexts, features excellent specificity, high sensitivity, two-photon excitability, and ready BBB penetrability. Application of this probe to track in situ generation of $ONOO^-$ in the brains of live mice has provided direct evidence that vascular occlusion or laser irradiation would induce local $ONOO^-$ formation in injured cerebral microvessels. The probe should serve as a powerful imaging tool to explore $ONOO^-$ biology under a variety of pathological contexts in vitro and in vivo. Furthermore, electronic and steric effects on probe sensitivity and the significance of probe pharmacokinetic properties to its real-world application, as considered in this work, should be instructive for future probe design.

ASSOCIATED CONTENT

Supporting Information

The Supporting Information is available free of charge on the ACS Publications website at DOI: 10.1021/jacs.5b06865.

General experimental details for chemistry, photophysical property characterization, and biology materials and methods; probe synthesis and structure characterization (Scheme S1); preparation of various ROS and RNS species; determination of quantum yield and two-photon absorption cross section; photophysical property data (Table S1 and Figures S1−S13); supplementary imaging (Figures S14−S27); and ^{1}H NMR, ^{13}C NMR, and HRMS spectra of **NP2**, **NP3**, and **NP4** (PDF)

Movie 1, showing that dynamic elevation of local $ONOO^-$ formation in the microvessel, indicated by

DOI: 10.1021/jacs.5b06865
J. Am. Chem. Soc. XXXX, XXX, XXX−XXX

strong **NP3** fluorescence, was efficiently monitored over a recording period of 30 s (AVI)

Movie 2, showing that endogenous $ONOO^-$ formation increased dramatically upon laser irradiation-mediated microvessel injury at 10 s point and remained at its highest fluorescent intensity for at least 30 s (AVI)

AUTHOR INFORMATION

Corresponding Authors

*changhuahan@zju.edu.cn (F.H.)
*huyz@zju.edu.cn (Y.-Z.H.)
*yhhu@mail.shcnc.ac.cn (Y.-H.H.)

Author Contributions

‖X.L. and R.-R.T contributed equally to this work.

Notes

The authors declare no competing financial interest.

ACKNOWLEDGMENTS

This work was supported in part by Projects of National Natural Science Foundations of China (81120108023, 81302748, 81300991, 81225022).

REFERENCES

(1) Radi, R. *J. Biol. Chem.* **2013**, *288*, 26464.
(2) Weidinger, A.; Kozlov, A. V. *Biomolecules* **2015**, *5*, 472.
(3) Ascenzi, P.; di Masi, A.; Sciorati, C.; Clementi, E. *Biofactors* **2010**, *36*, 264.
(4) Franco, M. C.; Estévez, A. G. *Cell. Mol. Life Sci.* **2014**, *71*, 3939.
(5) Szabó, C.; Ischiropoulos, H.; Radi, R. *Nat. Rev. Drug Discovery* **2007**, *6*, 662.
(6) Ferrer-Sueta, G.; Radi, R. *ACS Chem. Biol.* **2009**, *4*, 161.
(7) Pacher, P.; Beckman, J. S.; Liaudet, L. *Physiol. Rev.* **2007**, *87*, 315.
(8) Turko, I. V.; Murad, F. *Pharmacol. Rev.* **2002**, *54*, 619.
(9) Wilcox, C. S.; Pearlman, A. *Pharmacol. Rev.* **2008**, *60*, 418.
(10) Han, F.; Shirasaki, Y.; Fukunaga, K. *J. Neurochem.* **2006**, *99*, 97.
(11) Han, F.; Chen, Y. X.; Lu, Y. M.; Huang, J. Y.; Zhang, G. S.; Tao, R. R.; Ji, Y. L.; Liao, M. H.; Fukunaga, K.; Qin, Z. H. *J. Pineal Res.* **2011**, *51*, 124.
(12) Tao, R. R.; Wang, H.; Hong, L. J.; Huang, J. Y.; Lu, Y. M.; Liao, M. H.; Ye, W. F.; Lu, N. N.; Zhu, D. Y.; Huang, Q.; Fukunaga, K.; Lou, Y. J.; Shoji, I.; Wilcox, C. X.; Lai, E. Y.; Han, F. *Antioxid. Redox Signaling* **2014**, *21*, 1.
(13) Cross, A. H.; Manning, P. T.; Stern, M. K.; Misko, T. P. *J. Neuroimmunol.* **1997**, *80*, 121.
(14) Nadler, A.; Schultz, C. *Angew. Chem., Int. Ed.* **2013**, *52*, 2408.
(15) Ueno, T.; Nagano, T. *Nat. Methods* **2011**, *8*, 642.
(16) Kobayashi, H.; Ogawa, M.; Alford, R.; Choyke, P. L.; Urano, Y. *Chem. Rev.* **2010**, *110*, 2620.
(17) Yang, Y.; Zhao, Q.; Feng, W.; Li, F. *Chem. Rev.* **2013**, *113*, 192.
(18) Domaille, D. W.; Que, E. L.; Chang, C. J. *Nat. Chem. Biol.* **2008**, *4*, 168.
(19) Guo, Z.; Park, S.; Yoon, J.; Shin, I. *Chem. Soc. Rev.* **2014**, *43*, 16.
(20) Denk, W.; Strickler, J. H.; Webb, W. W. *Science* **1990**, *248*, 73.
(21) Wang, K. H.; Majewska, A.; Schummers, J.; Farley, B.; Hu, C.; Sur, M.; Tonegawa, S. *Cell* **2006**, *126*, 389.
(22) Arnon, T. I.; Horton, R. M.; Grigorova, I. L.; Cyster, J. G. *Nature* **2013**, *493*, 684.
(23) Both APF and HPF are commercially available from Invitrogen.
(24) Setsukinai, K.; Urano, Y.; Kakinuma, K.; Majima, H. J.; Nagano, T. *J. Biol. Chem.* **2003**, *278*, 3170.
(25) Zhou, X.; Kwon, Y.; Kim, G.; Ryu, J. H.; Yoon, J. *Biosens. Bioelectron.* **2015**, *64*, 285.
(26) Peng, T.; Wong, N. K.; Chen, X.; Chan, Y. K.; Ho, D. H.; Sun, Z.; Hu, J. J.; Shen, J.; El-Nezami, H.; Yang, D. *J. Am. Chem. Soc.* **2014**, *136*, 11728.
(27) Hou, J. T.; Yang, J.; Li, K.; Liao, Y. X.; Yu, K. K.; Xie, Y. M.; Yu, X. Q. *Chem. Commun.* **2014**, *50*, 9947.
(28) Chen, Z. J.; Ren, W.; Wright, Q. E.; Ai, H. W. *J. Am. Chem. Soc.* **2013**, *135*, 14940.
(29) Lin, K. K.; Wu, S. C.; Hsu, K. M.; Hung, C. H.; Liaw, W. F.; Wang, Y. M. *Org. Lett.* **2013**, *15*, 4242.
(30) Yu, F.; Li, P.; Wang, B.; Han, K. *J. Am. Chem. Soc.* **2013**, *135*, 7674.
(31) Zhang, Q.; Zhu, Z.; Zheng, Y.; Cheng, J.; Zhang, N.; Long, Y. T.; Zheng, J.; Qian, X.; Yang, Y. *J. Am. Chem. Soc.* **2012**, *134*, 18479.
(32) Yu, F.; Li, P.; Li, G.; Zhao, G.; Chu, T.; Han, K. *J. Am. Chem. Soc.* **2011**, *133*, 11030.
(33) Peng, T.; Yang, D. *Org. Lett.* **2010**, *12*, 4932.
(34) Zielonka, J.; Sikora, A.; Joseph, J.; Kalyanaraman, B. *J. Biol. Chem.* **2010**, *285*, 14210.
(35) Sun, Z. N.; Wang, H. L.; Liu, F. Q.; Chen, Y.; Tam, P. K.; Yang, D. *Org. Lett.* **2009**, *11*, 1887.
(36) Yang, D.; Wang, H. L.; Sun, Z. N.; Chung, N. W.; Shen, J. G. *J. Am. Chem. Soc.* **2006**, *128*, 6004.
(37) Ueno, T.; Urano, Y.; Kojima, H.; Nagano, T. *J. Am. Chem. Soc.* **2006**, *128*, 10640.
(38) Lou, Z.; Li, P.; Han, K. *Acc. Chem. Res.* **2015**, *48*, 1358.
(39) Chan, J.; Dodani, S. C.; Chang, C. J. *Nat. Chem.* **2012**, *4*, 973.
(40) Lemke, E. A.; Schultz, C. *Nat. Chem. Biol.* **2011**, *7*, 480.
(41) Mathis, C. A.; Wang, Y.; Holt, D. P.; Huang, G. F.; Debnath, M. L.; Klunk, W. E. *J. Med. Chem.* **2003**, *46*, 2740.
(42) Woolfe, G. J.; Melzig, M.; Schneider, S.; Dorr, F. *Chem. Phys.* **1983**, *77*, 213.
(43) So, P. T. C. Two-photon Fluorescence Light Microscopy. In *Encyclopedia of Life Sciences*; Macmillan Publishers Ltd, Nature Publishing Group, 2002.
(44) Albota, M. A.; Xu, C.; Webb, W. W. *Appl. Opt.* **1998**, *37*, 7352.
(45) Data in agreement with reported: Pierens, G. K.; Venkatachalam, T. K.; Reutens, D. *Magn. Reson. Chem.* **2014**, *52*, 453.
(46) Dugo, L.; Serraino, I.; Fulia, F.; De Sarro, A.; Caputi, A. P.; Cuzzocrea, S. *J. Pineal Res.* **2001**, *31*, 76.
(47) Teixeira, A.; Morfim, M. P.; de Cordova, C. A. S.; Charão, C. C. T.; de Lima, V. R.; Creczynski-Pasa, T. B. *J. Pineal Res.* **2003**, *35*, 262.
(48) Yin, J.; Liu, Y. H.; Xu, Y. F.; Zhang, Y. J.; Chen, J. G.; Shu, B. H.; Wang, J. Z. *J. Pineal Res.* **2006**, *41*, 124.
(49) Han, F.; Tao, R. R.; Zhang, G. S.; Lu, Y. M.; Liu, L. L.; Chen, Y. X.; Lou, Y. J.; Fukunaga, K.; Hong, Z. H. *J. Pineal Res.* **2011**, *50*, 281.
(50) Indo, H. P.; Yen, H. C.; Nakanishi, I.; Matsumoto, K.; Tamura, M.; Nagano, Y.; Matsui, H.; Gusev, O.; Cornette, R.; Okuda, T.; Minamiyama, Y.; Ichikawa, H.; Suenaga, S.; Oki, M.; Sato, T.; Ozawa, T.; Clair, D. K.; Majima, H. J. *J. Clin. Biochem. Nutr.* **2015**, *56*, 1.
(51) Bharath, S.; Andersen, J. K. *Antioxid. Redox Signaling* **2005**, *7*, 900.
(52) Tripathi, D. N.; Chowdhury, R.; Trudel, L. J.; Tee, A. R.; Slack, R. S.; Walker, C. L.; Wogan, G. N. *Proc. Natl. Acad. Sci. U. S. A.* **2013**, *110*, E2950.
(53) Liu, Q. B.; Liu, L. L.; Lu, Y. M.; Tao, R. R.; Huang, J. Y.; Shioda, N.; Moriguchi, S.; Fukunaga, K.; Han, F.; Lou, Y. J. *Toxicol. Appl. Pharmacol.* **2010**, *244*, 374.
(54) Schaffer, C. B.; Friedman, B.; Nishimura, N.; Schroeder, L. F.; Tsai, P. S.; Ebner, F. F.; Lyden, P. D.; Kleinfeld, D. *PLoS Biol.* **2006**, *4*, e22.
(55) Nishimura, N.; Schaffer, C. B.; Friedman, B.; Tsai, P. S.; Lyden, P. D.; Kleinfeld, D. *Nat. Methods* **2006**, *3*, 99.

DOI: 10.1021/jacs.5b06865
J. Am. Chem. Soc. XXXX, XXX, XXX−XXX